arXiv:1604.07469v2 [nucl-ex] 12 Aug 2016

Triangular flow of negative pions emitted in PbAu collisions at $\sqrt{s_{NN}}$ = 17.3 GeV*

D. Adamová[a], G. Agakichiev[b,l], A. Andronic[c,m], D. Antończyk[d], H. Appelshäuser[d], V. Belaga[b], J. Bielčíková[e,f,n], P. Braun-Munzinger[c,m], O. Busch[f], A. Cherlin[g], S. Damjanović[f], T. Dietel[h,t], L. Dietrich[f], A. Drees[i], W. Dubitzky[f], S. I. Esumi[f,o], K. Filimonov[f,p], K. Fomenko[b], Z. Fraenkel[g,*], C. Garabatos[c], P. Glässel[f], G. Hering[c], J. Holeczek[c], M. Kalisky[c], Iu. Karpenko[k,u], G. Krobath[f], V. Kushpil[a], A. Maas[c], A. Marín[c,m], J. Milošević[f,q,**], D. Miśkowiec[c,m], Y. Panebrattsev[b], O. Petchenova[b], V. Petráček[f,r], S. Radomski[c], J. Rak[c,s], I. Ravinovich[g], P. Rehak[j,*], H. Sako[c], W. Schmitz[f], S. Schuchmann[d], S. Sedykh[c], S. Shimansky[b], J. Stachel[f], M. Šumbera[a], H. Tilsner[f], I. Tserruya[g], G. Tsiledakis[c], J. P. Wessels[h], T. Wienold[f], J. P. Wurm[e], S. Yurevich[f,c], V. Yurevich[b]

[a]*Nuclear Physics Institute, Academy of Sciences of the Chech Republic, 25068 Řež, Czech Republic*
[b]*Joint Institute of Nuclear Research, Dubna, 141980 Moscow Region, Russia*
[c]*Institut für Kernphysik, GSI, 64291 Darmstadt, Germany*
[d]*Institut für Kernphysik, Johann Wolfgang Goethe-Universität Frankfurt, 60438 Frankfurt, Germany*
[e]*Max-Planck-Institut für Kernphysik, 69117 Heidelberg, Germany*
[f]*Physikalisches Institut, Universität Heidelberg, 69120 Heidelberg, Germany*
[g]*Department of Particle Physics, Weizmann Institute, Rehovot, 76100 Israel*
[h]*Institut für Kernphysik, Universität Münster, 48149 Münster, Germany*
[i]*Department for Physics and Astronomy, SUNY Stony Brook, NY 11974, USA*
[j]*Instrumentation Division, Brookhaven National Laboratory, Upton, NY 11973-5000, USA*
[k]*Frankfurt Institute for Advanced Studies, Ruth-Moufang-Straße 1, D-60438 Frankfurt am Main, Germany*
[l]*Present affiliation: II. Physikalisches Institut der Justus Liebig Universität, 35392 Giessen, Germany*
[m]*Present affiliation: Research Division and Extreme Matter Institute (EMMI), GSI Helmholtzzentrum für Schwerionenforschung, 64291 Darmstadt, Germany*
[n]*Present affiliation: Nuclear Physics Institute, Academy of Sciences of the Czech Republic, 25068 Řež, Czech Republic*
[o]*Present affiliation: Institute of Physics, University of Tsukuba, Tsukuba, Japan*
[p]*Present affiliation: Physics Department, University of California, Berkeley, CA 94720-7300, USA*
[q]*Present affiliation: University of Belgrade, Faculty of Physics and Vinča Institute of Nuclear Sciences, 11001 Belgrade, Serbia*
[r]*Present affiliation: Faculty of Nuclear Science and Engineering, Czech Technical University, 16636 Prague, Czech Republic*
[s]*Present affiliation: Department of Physics, University of Jyväskylä, Jyväskylä, Finland*
[t]*Present affiliation: Department of Physics, University of Cape Town, Rondebosch 7701, South Africa*
[u]*Present affiliation: INFN - Sezione di Firenze, Via G. Sansone 1, I-50019 Sesto Fiorentino (Firenze), Italy*

Abstract

Differential triangular flow, $v_3(p_T)$, of negative pions is measured at $\sqrt{s_{NN}}$= 17.3 GeV around midrapidity by the CERES/NA45 experiment at CERN in central PbAu collisions in the range 0-30% with a mean centrality of 5.5%. This is the first measurement as a function of transverse

momentum of the triangular flow at SPS energies. The p_T range extends from about 0.05 GeV/c to more than 2 GeV/c. The triangular flow magnitude, corrected for the HBT effects, is smaller by a factor of about 2 than the one measured by the PHENIX experiment at RHIC and the ALICE experiment at the LHC. Within the analyzed range of central collisions no significant centrality dependence is observed. The data are found to be well described by a viscous hydrodynamic calculation combined with an UrQMD cascade model for the late stages.

Keywords: Triangular flow, SPS, heavy-ion
PACS: 25.75.Ld

[☆] CERES Collaboration
[*] *deceased*
[**] corresponding author
Email address: Jovan.Milosevic@cern.ch (J. Milošević)

1. Introduction

The azimuthal anisotropy of particles emitted in heavy-ion collisions is used to study properties of hot and dense systems created in such collisions. The almond shape of the overlapping region in a non-central collision manifests itself in the appearance of the elliptic flow anisotropy (1) driven by strong interactions among constituents of the expanding medium. By these interactions the geometrical anisotropy of the overlap zone evolves, following the pressure gradients, into the momentum space anisotropy that is measured by the second harmonic coefficient v_2. But due to fluctuating positions of the colliding nucleons, the event plane derived from the elliptic anisotropy is not a strict plane of symmetry, and higher-order anisotropies may appear (2). In fact, among the prominent results from collider experiments are observations of significant triangular flow, at the Relativistic Heavy Ion Collider (RHIC) at nucleon-nucleon center-of-mass energy up to $\sqrt{s_{\rm NN}}$ = 200 GeV (3, 4, 5), and at the Large Hadron Collider (LHC) at $\sqrt{s_{\rm NN}}$ = 2.76 TeV (7, 8, 9), both in central and non-central collisions.

The large v_2 values of collective flow agree well with predictions of relativistic hydrodynamics (10) without dissipation. This suggests that elliptic flow is developed in the early phase of a locally equilibrated, strongly interacting Quark Gluon Plasma (QGP). The QGP behaves as a nearly perfect liquid with a very small ratio η/s of shear viscosity to entropy density, close to its string-theoretical limit of $1/4\pi$ (11, 12).

The average elliptic flow magnitude, v_2, is about 20% larger at the LHC compared to RHIC (13, 14, 15). This increase is mainly due to the harder $p_{\rm T}$ spectrum at LHC energies. The measured v_2 is in agreement with hydrodynamical extrapolations from RHIC data using the same η/s value (16, 17) and also in agreement with a hybrid calculation treating the QGP by ideal hydrodynamics and the late stages by a hadronic cascade model (18). Contrary to the elliptic flow, the triangular flow is nearly independent of centrality. The triangular flow can be described using viscous hydrodynamics and transport models. Triangular flow is found to be a sensitive probe of initial geometry fluctuations and viscosity (19).

The elliptic flow magnitude v_2 measured at the Super Proton Synchrotron (SPS) energy, $\sqrt{s_{\rm NN}}$ = 17.3 GeV, is about 30% lower than those at the top RHIC energy of $\sqrt{s_{\rm NN}}$ = 200 GeV (3). Except for the most central collisions (20), the differential flow data $v_2(p_{\rm T})$ at SPS (21, 22, 23), although very similar in shape to the RHIC and LHC data, stay below calculations of ideal hydrodynamics (24). This failure of ideal hydrodynamics at the top SPS energy has been ascribed to insufficient number densities at very early collision stages (25) and strong dissipative effects at the late hadronic stages (11, 12, 26, 27).

In this paper, we present the first measurement of triangular flow at SPS energy. Experimental results comprise differential triangular flow $v_3(p_{\rm T})$ of negative pions emitted from central 158 *A*GeV PbAu collisions. The results are compared with the measurement of the triangular flow performed by the PHENIX collaboration at RHIC and the ALICE Collaboration at LHC and also with a hydrodynamics calculation coupled with a UrQMD cascade model (28) to describe the late stages. These findings might shed some light on the late stage of collective expansion characterized by rescattering in the 'hadronic corona' (29).

2. Experiment and data sample

A sample of $30 \cdot 10^6$ central PbAu events was collected with the upgraded CERES/NA45 spectrometer during the heavy-ion run at the top SPS energy of 158 *A*GeV. Within the polar angle acceptance of $7.7^\circ < \vartheta < 14.7^\circ$, which corresponds to a pseudorapidity range $2.05 < \eta < 2.70$ near midrapidity ($y_{\mathrm{mid}} = 2.91$), the CERES spectrometer has axial symmetry around the beam direction. As it covers the full azimuth ϕ, it is very suitable for studies of azimuthal anisotropy. A detailed description of the CERES experiment is given in (30).

A precise momentum determination is provided by the radial-drift Time Projection Chamber (TPC) (31) which is operated inside an axially symmetric magnetic field with a radial component providing deflection in r_ϕ. Negative pions are identified using the differential energy loss dE/dx along their tracks in the TPC. For vertex reconstruction and tracking outside the magnetic field, two radial Silicon Drift Detectors (SDD) (32) are placed at 10 and 13 cm downstream of a segmented Au target. Negative pions are reconstructed by matching track segments in the SDD doublet and in the TPC using a momentum-dependent matching window. Depending on pion momentum, the relative momentum resolution varies between 2% and 8%.

A mix of three triggers designed to enhance central events has been used for data collection in the range 0 – 30% of $\sigma/\sigma_{\mathrm{geo}}$ with an average centrality of 5.5% in the data sample. The track-multiplicity distribution for all triggers combined ('all triggers') is shown in Fig. 1 by full black

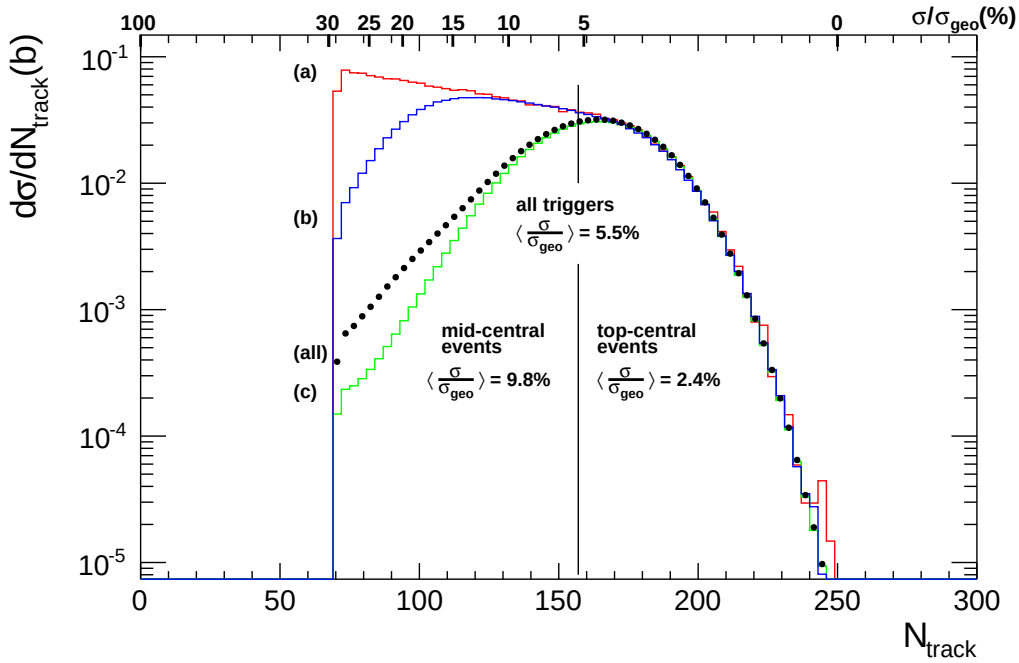

Figure 1: TPC track density for our trigger mix within (0 – 30%) centrality. The distribution consists of several components: (a) minimum-bias (0.5%), (b) semicentral (8.3%), and (c) central (91.2%), where the parenthesis represent the percentage fractions in the mix. The mix of all triggers, with a resulting mean centrality of 5.5 %, is labeled 'all triggers' and displayed by black circles. The vertical axis represents the differential cross-section expressed in barns (b). The $\langle \sigma/\sigma_{geo} \rangle$ axis on top applies to minimum-bias data only.

symbols. At low multiplicities, it strongly deviates from the minimum-bias distribution labeled (*a*). Beside minimum-bias data, which contribute 0.5%, a semi-central trigger, labeled (*b*), contributes 8.3 % to the total. The biggest share of data, 91.2%, is collected with a most central trigger labeled (*c*) in Fig. 1. Note that the data will be presented here, besides 'all triggers', for 'top-central' and 'mid-central' triggers by selecting $N_{track} > 159$ or ≤ 159, with weighted mean centralities of 2.4% and 9.8%, respectively. We remark that because of the unconventional shape of the 'all triggers' and 'mid-central' distributions, we have supplied the actual distributions in digitized form for theory comparisons.

3. Analysis and results

Among the higher-order harmonics, the triangular collective flow is of particular interest. It is quantified by v_3, the third-order harmonic coefficient of the azimuthal particle distribution measured with respect to Ψ_3, the azimuthal angle of the 3rd-order participant event-plane. The angle Ψ_3 is determined as:

$$\Psi_3 = \frac{1}{3}\arctan\frac{\sum_{i=0}^{n} w_i(p_{Ti})\sin(3\phi_i)}{\sum_{i=0}^{n} w_i(p_{Ti})\cos(3\phi_i)}. \quad (1)$$

Here, ϕ_i is the azimuthal angle of the i-th particle out of n used for event-plane reconstruction, and $w_i(p_{Ti})$ are weights used to optimize the event-plane resolution. In the same way as in (20), the ϕ coordinates are divided into 100 adjacent equal slices spanning the full azimuth. This ap-

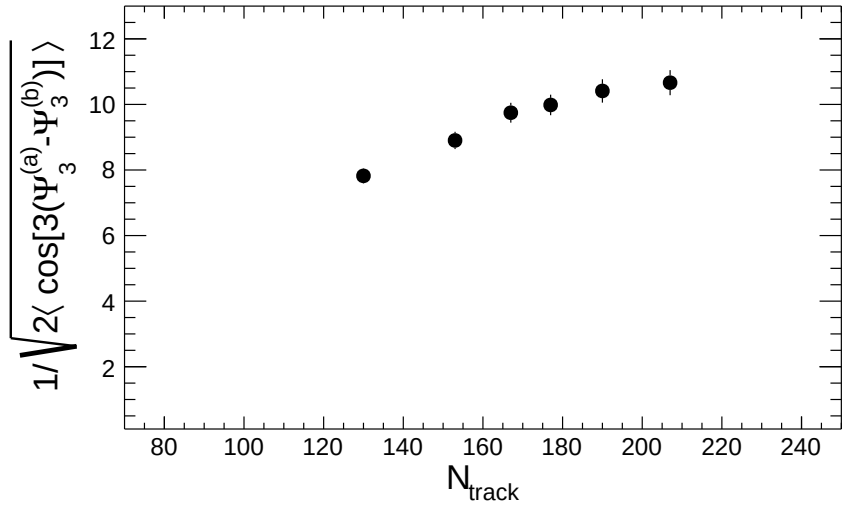

Figure 2: The correction factor of the 3rd-order event plane as a function of TPC multiplicity for the 2-subevents method (pion data).

proach is used to avoid the trivial autocorrelation effect, and some contribution from short-range correlations. In order to correct for local detector inefficiency, a shifting and flattening procedure has been applied (for more details see (33)) to ensure an azimuthally isotropic event-plane distribution. The azimuthal anisotropy of particle tracks is then measured with respect to the 3rd-order event plane reconstructed by employing tracks from non-adjacent slices only. The finite resolution of the event plane orientation is obtained from the differences between the event planes reconstructed from two sliced subevents, a and b. The corresponding correction factor is calculated as $(2\langle\cos[3(\Psi_3^{(a)} - \Psi_3^{(b)})]\rangle)^{-1/2}$, and used to compensate the raw v_3 for finite event-plane resolution. As the latter depends on multiplicity, the correction factor is calculated for different centralities. Both, the event multiplicity and the v_3 magnitude influence the event-plane resolution. Fig. 2 shows that a decrease of the dispersion in event-plane orientation with increasing multiplicity is weaker than

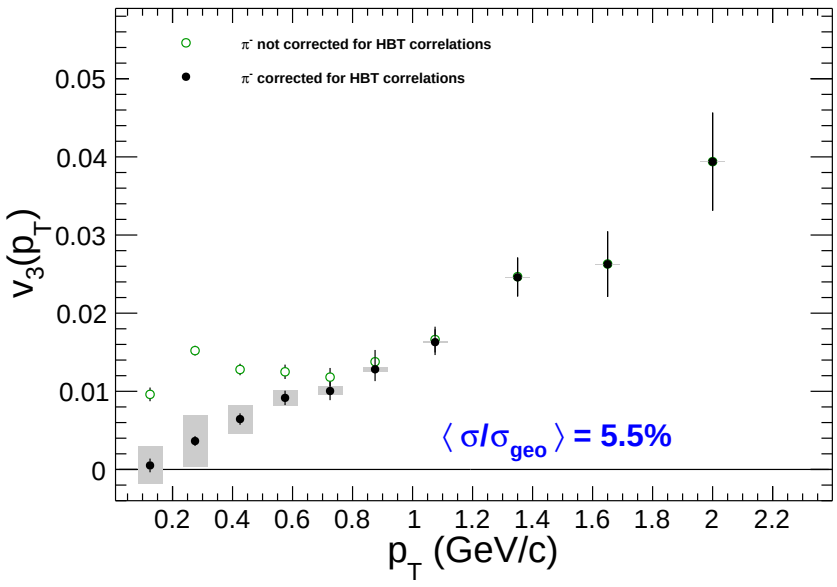

Figure 3: The magnitude v_3 of triangular flow as a function of negative pion transverse momentum before (open green circles) and after (closed circles) correcting for the HBT effect. 'All triggers', averaged centrality 5.5%. Statistical uncertainties are represented with the error bars, while systematic ones are indicated by gray rectangles.

the decrease in anisotropy. In order to reduce statistical errors, the v_3 results, presented in this paper, are obtained by merging the results obtained in six narrower multiplicity bins.

Since almost all particles accepted for analysis are negative pions, subsamples become partially correlated due to the Hanbury Brown & Twiss effect (HBT) of identical bosons. This effect produces a space-momentum correlation between two pions of the same charge if the product of their momentum difference and the source radius R is below the uncertainty limit, i.e., $|\vec{p}_2 - \vec{p}_1| \leq \hbar/R$. In the rather central collisions under study here, R is typically 7 fm, and consequently $\hbar/R \approx 30$ MeV/c, much smaller than the mean pion momentum $\langle p_{\mathrm{T}} \rangle \approx 400$ MeV/c. Moreover, the HBT correlation is short range also in azimuth, and it is significant only if $|\phi_1 - \phi_2| \leq \hbar/Rp_{\mathrm{T}} \simeq 0.1$. As we deal with bosons, the correlation is positive like flow itself, and therefore applying the flow analysis to the HBT correlations would result in a spurious flow.

In order to subtract the non-flow HBT contribution we follow (34, 35) and use the standard Bertsch-Pratt parametrization in the comoving system. The corresponding parameters R_{side}, R_{out}, R_{long} describe the dimensions of the source and the so-called chaoticity parameter λ their degree of non-coherence. λ is allowed to be varied by generous ±50% to account for different track resolution in TPC and the SDD doublet; the former is used for the determination of the source parameters, the latter for the event plane determination. The numerical values R_{side}, R_{out}, R_{long} and λ are obtained from the CERES HBT data (36, 37, 38) by averaging over $k_t \leq 0.6$ GeV/c.

As expected, the size of the corrections applied to the data displayed in Fig. 3 is quite large at low p_{T}, but decreases rapidly with increasing p_{T}. The systematic uncertainty in the HBT contribution is derived by calculating the correction varying all source parameters by ±1 σ together and independently, and then taking the error of the mean of the resulting distribution to represent the

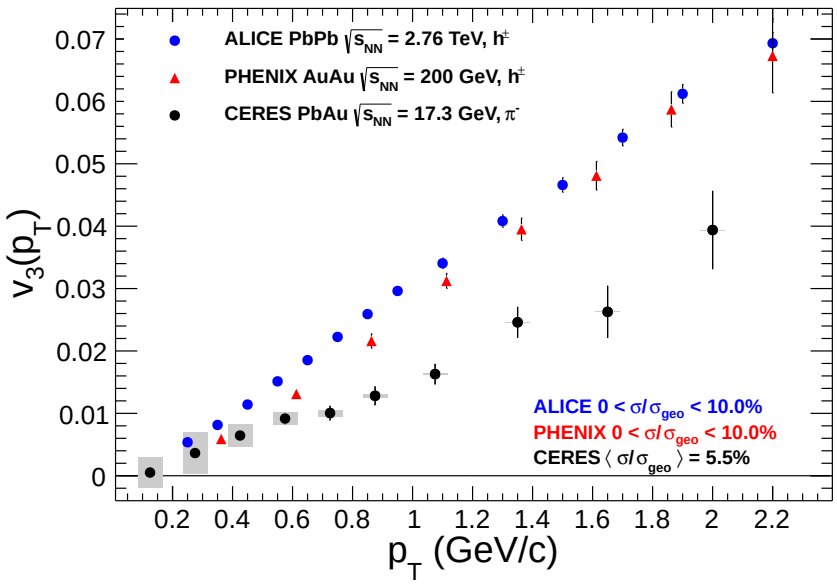

Figure 4: Comparison of triangular flow v_3 of negative pions *vs* p_T: from PbAu collisions at $\sqrt{s_{\rm NN}}$ = 17.3 GeV (CERES, solid black circles); from AuAu collisions at $\sqrt{s_{\rm NN}}$ = 200 GeV (PHENIX, red triangles); from PbPb collisions at $\sqrt{s_{\rm NN}}$ = 2.76 TeV (ALICE, solid blue circles) at comparable centrality. Statistical uncertainties are represented with the error bars, while systematic uncertainties of the CERES results are indicated by gray rectangles.

systematic uncertainty in each bin.

The systematic uncertainties in the corrected v_3 have significant size (up to 0.4%) just in the p_T region where the HBT effect is greatest. They become negligible for p_T approaching 0.8 GeV/c. In order to stabilize the final HBT-corrected value of the triangular flow, several iterations of the correction procedure described in (34) have been performed until the difference between the final HBT-corrected v_3 value and the one before it became smaller than 10^{-4}. The triangular flow values corrected this way increase about linearly, starting from zero at transverse momenta close to zero up to 0.04 at p_T around 2 GeV/c.

Fig. 4 compares our triangular flow results with those from the PHENIX and ALICE Collaborations at $\sqrt{s_{\rm NN}}$ = 200 GeV and $\sqrt{s_{\rm NN}}$ = 2.76 TeV (3, 39), respectively, in the limited $p_{\rm T}$ range accessible to CERES and at comparable centrality.

By inspection of Fig. 4 we conclude that the magnitudes of triangular flow at RHIC and at LHC energy are nearly equal (40). In contrast, the magnitude at the top SPS energy reaches only about one half of the corresponding value at LHC energy. The transverse momentum range of the analyzed SPS data is small with respect to that covered by ALICE data (39). In this restricted p_T range the data suggest a linear $v_3(p_{\rm T})$ dependence starting from zero.

We like to remark that ALICE uses large gaps in pseudo-rapidity between tracks used for event-plane reconstruction and tracks to measure v_3; this way non-flow contributions from jets and mini-jets might have been effectively suppressed. Although jet-like correlations have been observed at SPS energy (22) at the much lower $\sqrt{s_{\rm NN}}$ compared to LHC, the minijet density is strongly reduced. In Ref (22) it is shown that in very central PbAu collisions at SPS energies

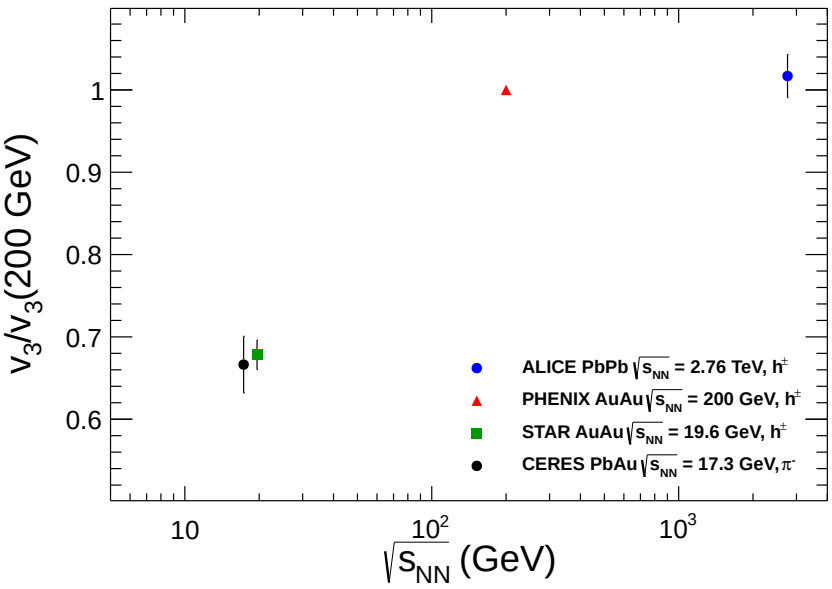

Figure 5: Ratios of the triangular flow v_3 measured at different collision energies with respect to the v_3 magnitude measured at PHENIX AuAu collisions at $\sqrt{s_{\mathrm{NN}}}$ = 200 GeV. The v_3 are obtained by integrating the corresponding differential $v_3(p_T)$ over $0.3 < p_T < 2.1$ GeV/c. The data from ALICE, PHENIX and STAR were taken from (5), (3) and (39) respectively.

the total jet yield is about 0.02 per event which is more than an order of magnitude smaller with respect to the corresponding yield at the LHC energy, while the charged particle pseudo-rapidity density is only 4 times smaller (41). This is quite fortunate, since to employ a pseudo-rapidity gap is no option for the limited acceptance in CERES.

On Fig. 3 in (5) is shown of the p_T-integrated two-particle Fourier coefficients, i.e. of the squared v_3 magnitude as a function of $\sqrt{s_{NN}}$ energy with a shallow minimum between 10 and 20 GeV. The integration has been performed for $p_T > 0.2$ GeV/c. The ratio between the v_3 at 19.6 GeV, which is quite close to the top SPS energy of 17.3 GeV/c, with respect to the v_3 measured at 200 GeV is about 0.63. In Fig. 5 are depicted corresponding ratios for 17.3, 19.6, 200 and 2760 GeV/c where the p_T integration has been done within the range $0.3 < p_T < 2.1$ GeV/c. The v_3 ratio between the top SPS and the top RHIC energy is about 0.66 which is quite close to the one found in (5). This is alo in a rather good agreement with an AMPT predictions from (6) for the ratio of about 0.6.

In contrast to elliptic flow which reflects the initial anisotropy of the fireball and thus depends strongly on centrality (see Fig. 24 in (20) and Fig. 6.22 in (33)), triangular flow arises entirely from fluctuations of the initial shape, and we see from Fig. 6 that its magnitude is not significantly different for mid-central and top-central collisions, with mean averaged centralities of 2.4% and 9.8%, respectively. A rather weak centrality dependence has also been reported by ALICE (see Fig. 1 in (39, 40)) where a very slight increase of v_3 with centrality has been observed. The different centrality behaviour of elliptic and triangular flow can also be observed from the corresponding p_{T}-dependencies displayed in Fig. 7. The systematic errors of the v_3 data shown in Fig. 6 and

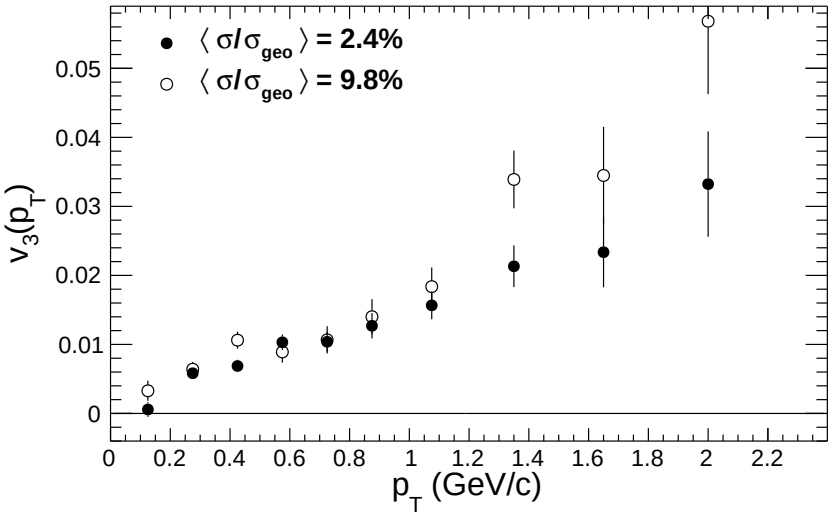

Figure 6: Triangular flow $v_3(p_T)$ at two different mean centralities, at top-central (closed circles) and at mid-central (open circles) collisions.

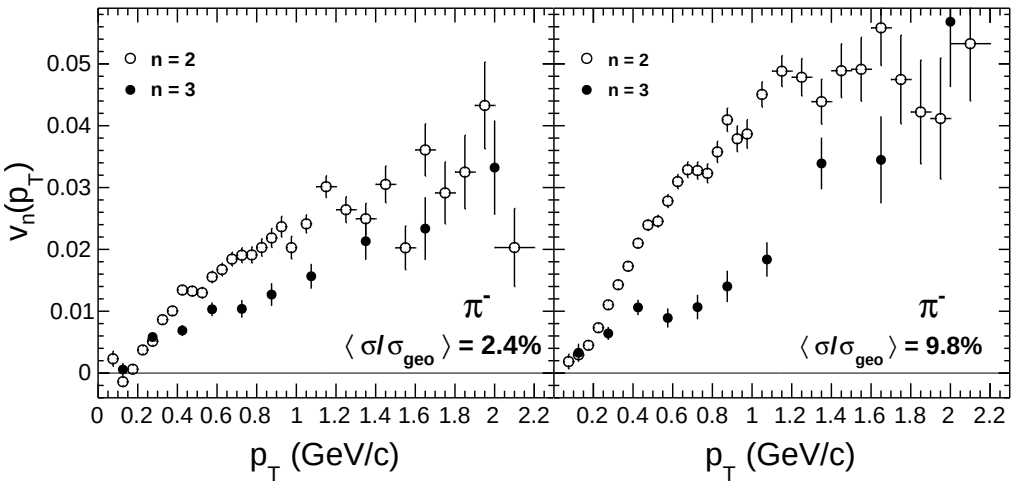

Figure 7: Elliptic and triangular flow magnitudes, $v_2(p_T)$ (open circles) and $v_3(p_T)$ (closed circles), respectively, for top-central (left panel) and mid-central collisions (right panel).

Fig. 7 are very similar to those found for mean centrality of 5.5%.

Approaches combining the relativistic hydrodynamics with transport models (so-called hybrid models) have been applied to describe the expansion stage of heavy-ion collisions at ultra-relativistic energies. In such models viscous or ideal fluid dynamics is used to describe the evo-

lution of the hot and dense quark-gluon plasma, and hadron transport to describe the evolution of the late sparse hadron gas. The calculations shown here are done using a hybrid model (28) combining the vHLLE viscous hydrosolver (42) with UrQMD hadron cascade (43). In this model both kinetic and chemical freeze-outs are described dynamically by the UrQMD hadron cascade, and thus there are no clear freeze-out temperatures. With this approach, particle yields, in particular for strange mesons and baryons, are not well described. However, since we deal here with pions only, this may not be a serious shortcoming. The switch from fluid to cascade, the 'particlization' (28), is set to take place on a constant energy density surface where $\epsilon = 0.5$ GeV/fm^3. Since the net baryon density is not uniform on such a surface, this density does not correspond to a single temperature. Within the chiral model of the Equation of State (EoS) used in this hydrodynamics description, the value of the switching density ϵ_{sw} corresponds to $T \approx 175$ MeV at $\mu_B = 0$. The remaining parameters of the model are the two Gaussian radii for the initial distribution of energy, and the starting time for the hydrodynamic phase. Their values, together with the value of the switching density, $\epsilon_{sw} = 0.5$ GeV/fm^3, are based on reproduction of the data in collisions at RHIC energies, and are kept unchanged at the SPS for simplicity. In Ref. (28), the authors investigated parameter dependence of the model results in the case of 0-5% centrality AuAu collisions at $\sqrt{s_{NN}} = 19.6$ GeV. It is shown that the model results change less than 10% when the parameters of the model are varied by 10%. Within the model (28) is studied the dependence of the elliptic and triangular flow magnitude on the collision energy.

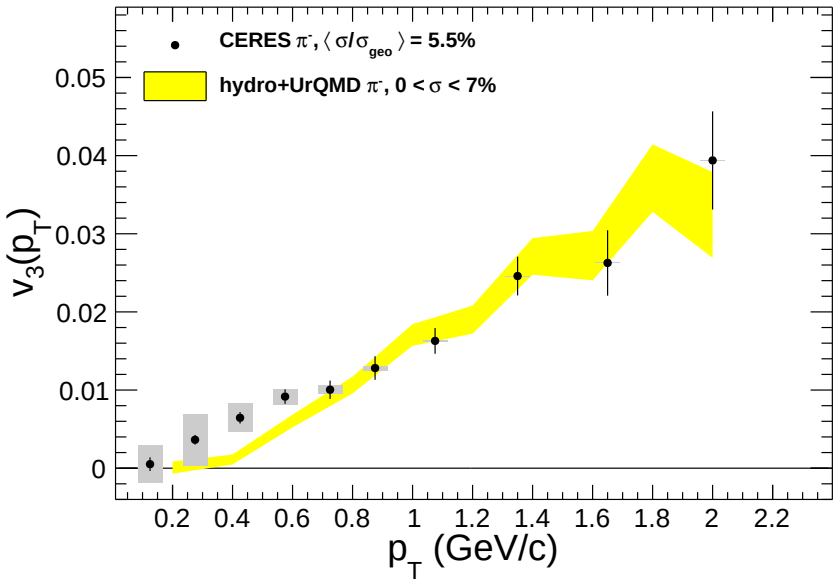

Figure 8: Comparison between the p_T dependence of negative pion v_3 measured in PbAu collisions at $\sqrt{s_{\rm NN}} = 17.3$ GeV with hydrosolver+UrQMD model predictions. The statistical errors of the model predictions are shown as yellow band. Statistical uncertainties of the experimental results are represented with the error bars, while systematic ones are indicated by gray rectangles.

In Fig. 8, the comparison between the predictions by this hydrosolver+UrQMD model and our $v_3(p_T)$ measurements of negative pions in PbAu collisions is shown. The model predictions

are calculated for hadrons within $0.2 < p_T < 2.0$ GeV/c and $-1 < \eta < 1$, which is very close to the experimental acceptance. Also, the centrality samples which roughly correspond to the experimental ones are simulated. Comparing the presented distributions, one can conclude that the model predictions are in a rather good agreement with the experimental results, except in the p_T region between 0.3 and 0.7 GeV/c where the model slightly underpredicts the experimental data.

4. Summary

The triangular flow appears as a hydrodynamic response of the system created in heavy-ion collision to the fluctuation of the positions of the overlapping nucleons at the moment of impact. In this paper, for the first time, results on the differential triangular flow $v_3(p_T)$ are presented measured at the top SPS energy. The magnitudes of v_3 are found to be about one half of the ones measured at the top RHIC and LHC energies. The v_3 measured by CERES at SPS energy of $\sqrt{s_{\rm NN}}$ = 17.3 GeV is similar to the one measured by STAR at RHIC energy of $\sqrt{s_{\rm NN}}$ = 19.6 GeV. The hydrosolver+UrQMD model is able to reproduce the experimental data rather well. This comparison could shed some light on the dynamics of the system created in heavy-ion collisions at top SPS energy.

5. Acknowledgments

We are grateful to Pasi Huovinen for his guidance concerning the hydrodynamical calculations to be compared to SPS data and appreciate his critical reading of the manuscript concerning the applied hydrosolver+UrQMD model. We acknowledge the support by the Ministry of Education, Science and Technological Development of the Republic of Serbia throughout the project 171019.

References

[1] J-Y. Ollitrault, Phys. Rev. **D 46**, 229 (1992).
[2] B. Alver and G. Roland, Phys. Rev. **C 81**, 054905 (2010).
[3] A. Adare *et al*., PHENIX Collaboration, Phys. Rev. Lett. **107**, 252301 (2011).
[4] X. Sun for the STAR Collaboration, Nucl. Phys. **A 931**, 1194 (2014).
[5] L. Adamczyk *et al*., STAR Collaboration, Phys. Rev. Lett. **116**, 112302 (2016).
[6] D. Solanki, P. Sorensen, S. Basu, R. Raniwala, and T. K. Nayak, Phys. Lett. **B720**, 352 (2013).
[7] K. Aamodt *et al*., ALICE Collaboration, Phys. Rev. Lett. **107**, 032301 (2011).
[8] G. Aad *et al*., ATLAS Collaboration, Phys. Rev. **C 86**, 014907 (2012).
[9] S. Chatrchyan *et al*., CMS Collaboration, Phys. Rev. **C 89**, 044906 (2014).
[10] P. Huovinen, P.V. Ruuskanen, Ann. Rev. Nucl. Part. Sci. **56**, 163 (2006).
[11] M. Gyulassy, L. McLerran, Nucl. Phys. **A 750**, 30 (2005).
[12] T. Hirano, U. Heinz, D. Kharzeev, R. Lacey, Y. Nara, Phys. Lett.**B 636**, 299 (2006).
[13] K. Aamodt *et al*., ALICE Collaboration, Phys. Rev. Lett. **105**, 252302 (2010).
[14] ATLAS Collaboration, arXiv:1108.6018.
[15] I. Tserruya, AIP Conf. Proc. 1422, 166 (2012), arXiv:1108.6018.
[16] M. Luzum, Phys. Rev.**C 83**, 044911 (2011).
[17] C. Shen, U. Heinz, P. Huovinen, H. Song, arXiv:nucl-th/1105.3226.
[18] T. Hirano, P. Huovinen, and Y. Nara, Phys. Rev. **C 83**, 021902 (2011).
[19] B. Alver, C. Gombeaud, M. Luzum and J.-Y. Ollitrault, Phys. Rev.**C 82**, 034913 (2010).
[20] D. Adamová *et al*., NA45/CERES Collaboration, Nucl. Phys. A **894**, 41 (2012).
[21] C. Alt *et al*., NA49 Collaboration, Phys. Rev. **C 68**, 034903 (2003).
[22] G. Agakichiev *et al*., NA45/CERES Collaboration, Phys. Rev. Lett. **92**, 032301 (2004).
[23] M.M. Aggarwal *et al*., WA98 Collaboration, Nucl. Phys. **A 762**, 129 (2005).
[24] P. Huovinen, P.F. Kolb, U. Heinz, P.V. Ruuskanen, S.A. Voloshin, Phys. Lett.**B 503**, 58 (2001).
[25] U. Heinz, P. Kolb,J. Phys. **G30**, S1229 (2004).
[26] D. Teaney, Phys. Rev. **C 68**, 034913 (2003).
[27] H. Niemi, G.S. Denicol, P. Huovinen, E. Molnar, D.H. Rischke, Phys. Rev. Lett. **106**, 212302 (2011).
[28] I. A. Karpenko, P. Huovinen, H. Petersen and M. Bleicher, Phys. Rev. C **91**, 064901 (2015).
[29] T. Hirano and M. Gyulassy, Nucl. Phys. **A 769**, 71 (2006).
[30] A. Marín *et al*., NA45/CERES Collaboration, J. Phys. **G30**, S709 (2004).
[31] D. Adamova *et al*., NA45/CERES Collaboration, Nucl. Instr. Meth. **A593**, 203 (2008).
[32] P. Holl, P. Rehak, F. Ceretto, U. Faschingbauer, J.P. Wurm, A. Castoldi, E. Gatti, Nucl. Instr. Meth. **A377**, 367 (1996).
[33] J. Milošević, Universität Heidelberg, *Doctoral Thesis*, 2006.
[34] P.M. Dinh, N. Borghini and J.-Y. Ollitrault, Phys. Lett. **B 477**, 51 (2000).
[35] J. Slivova (now Bielčíková), University of Heidelberg and University of Prague, *Doctoral Thesis*, (2003), unpublished.
[36] H. Tilsner, NA45/CERES Collaboration, Universität Heidelberg, *Doctoral Thesis*, 2002.
[37] D. Adamova *et al*., NA45/CERES Collaboration, Nucl. Phys. **A714**, 124 (2003).
[38] D. Adamová, NA45/CERES Collaboration, Phys. Rev. **C 78**, 064901 (2008).
[39] K. Aamodt *et al*., ALICE Collaboration, Phys. Lett. **B 719**, 18 (2013).
[40] C. Gale *et al*., Int. J. Mod. Phys. **A 28**, 1340011 (2013).
[41] K. Aamodt *et al*., ALICE Collaboration, Phys. Rev. Lett. **105**, 252301 (2010)
[42] I. Karpenko, P. Huovinen and M. Bleicher, Comput. Phys. Commun. **185**, 3016 (2014)
[43] S. A. Bass *et al.*, Prog. Part. Nucl. Phys. **41**, 255 (1998); M. Bleicher *et al.*, J. Phys. G **25**, 1859 (1999)